We are IntechOpen, the world's leading publisher of Open Access books Built by scientists, for scientists

6,900
Open access books available

185,000
International authors and editors

200M
Downloads

Our authors are among the

154
Countries delivered to

TOP 1%
most cited scientists

12.2%
Contributors from top 500 universities



WEB OF SCIENCE™

Selection of our books indexed in the Book Citation Index in Web of Science™ Core Collection (BKCI)

Interested in publishing with us?
Contact book.department@intechopen.com

Numbers displayed above are based on latest data collected.
For more information visit www.intechopen.com



Chapter

Using Optimization Algorithms in the Design of SRM

Petrushin Alexandr Dmitrievich,
Kashuba Alexandr Viktorovich
and Petrushin Dmitry Alexandrovich

IntechOpen

Abstract

Switched reluctance motors (SRM) are increasingly used in various industries and vehicles, in addition, in household appliances and in medical equipment. This chapter presents the results of research on the geometric optimization of the magnetic circuit of the switched reluctance motor (SRM) and optimization of the control algorithm. The developed optimization method of magnetic circuit geometry is based on the existing Monte Carlo method. It also allows finding global maxima and minima of an objective function. The main differences of the developed method are as follows: it includes the normal distribution and searches for the geometric shape of the rotor pole as smooth curves (the air gap is not necessarily constant). The problem of optimal control was solved using the Pontryagin's maximum principle. The initial conditions for the auxiliary functions were determined using the Newton-Raphson method. The recommendations on the practical implementation of the optimal control algorithm are given.

Keywords: switched reluctance motor, optimization, Monte Carlo method, magnetic circuit, random curve generation algorithm, optimal control algorithm, Newton-Raphson iteration method

IntechOpen

1. Introduction

The approaches used in the design of electric drives are more and more similar to the laws of nature evolution [1–3]. Thus, during the evolution of living organisms, the problem of reliable life support is solved with minimal expenditure of energy with a constant change in natural environmental conditions. The theory and practice of using modern electric drives increasingly give them the features of an intellectual approach. This makes it possible to maintain a high level of reliability and operate efficiency with changing external influences.

In the process of the electric drive synthesis, there is no ideal technical solution for the same terms of reference and formulated requirements (like the laws of nature evolution, there are many different variations).

When creating an electric drive, it is often necessary to make a compromise between a highly specialized technical solution for one specific device and a universal version for use in various fields.

When creating electric drives, the best technical solutions are obtained using optimization algorithms. It should be noted that a more general formulation of the problem and less restrictions provide better results.

There are significant difficulties for the optimization problem (including optimization of the magnetic circuit geometry and control optimization) for the following reason. The existing methods of designing the magnetic circuit of switched reluctance motor (SRM) do not fully take into account the drive control algorithm, since they are guided either by the nominal mode of operation or by some mode for a particular application. This is caused by uncertainty: if the algorithm is divided into time sections (within which the control actions are constant), many optimal variants of the magnetic circuit are obtained when solving the optimization problem. The number of optimal variants is equal to the number of time sections. That is, when controlling the drive, the extremum of the cost function (CF) will be obtained only if the magnetic circuit of the electric motor (magnetic core and winding) changes its configuration. But this is impossible now and in the near future. We have covered this problem in paper [4]. In the same paper, we proposed an algorithm for determining the only variant of the magnetic circuit of the traction motor when solving the optimization problem with varying control actions.

This chapter (Sections 2–5) presents the results of the optimization of the magnetic circuit of the motor using the Monte Carlo method. The Monte Carlo method was adapted to find the optimal geometric shape of the rotor pole as smooth curves (the air gap is not necessarily constant). To reduce the calculation time and ensure a high probability of obtaining a global extremum when performing an optimization by an improved method, a variable probability density of a random variable is used.

This chapter (Section 6) presents the results of solving a boundary problem of optimal SRM control. The cost function includes the square of the voltage applied to the stator winding.

Recommendations on the practical implementation of the optimal control algorithm are given (using the most common half-bridge power circuit and modern electronic components).

2. Development of an optimization algorithm for the SRM magnetic circuit

There are many different optimization methods: simplex method, Monte Carlo method, ant colony optimization algorithms, gradient descent, evolutionary algorithm, etc. [5, 6]. All of them are adapted for specific aims and make it possible to take into account the specific conditions inherent in a particular task.

As an optimization criterion, there may be different characteristics of the motor: average electromagnetic torque, torque ripple, efficiency, heat loss, and others (depending on the requirements of terms of reference). In multi-objective optimization, the objective function must be set using mathematical equations that take into account the priority of a certain criterion or use multi-objective optimization algorithms.

The developed optimization algorithm is based on the Monte Carlo method. Experience in designing SRM [4] shows that using this method to optimize the geometric dimensions of the magnetic circuit can significantly improve the performance of the motor compared to the results of the design without the use of optimization.

The Monte Carlo method allows finding the global extremum of the several CF variables. The essence of this method is as follows:

1. Setting limits for all optimized parameters.

2. A series of pseudorandom numbers is generated (uniform distribution of a random variable) and is performed within the specified limits for each optimized parameter.

3. CF value calculation.

Repeating steps 2 and 3 provides an extensive basis for establishing various relationships. By analyzing the data obtained, it is possible to know which parameter values provide the extremum of CF.

One of the advantages of the Monte Carlo method is that it guarantees with a fairly high probability that the global (not local) extremum of the cost function is found. But the main drawback is the need to perform a huge amount of CF calculations (hundreds, thousands, tens of thousands) to get an acceptable result. This leads to more time spent on optimization. Hence, SRM design lasts much longer. Even with a few numbers of optimized parameters, this disadvantage is very noticeable.

The algorithm developed on the basis of the Monte Carlo method makes it possible to find the global extremum of the CF with an accuracy sufficient for many practical problems in a relatively short time.

It is possible to reduce the time of optimization by generating random numbers near the coordinates of the global extremum.

The main difference of the developed algorithm is the generation of random numbers performed according to the Gaussian laws. Its probability density function is expressed as

$$f(x) = \frac{e^{-\frac{(x-\mu)^2}{2\sigma^2}}}{\sqrt{2\pi\sigma^2}}, \tag{1}$$

where μ is the expected value, σ is the standard deviation, and σ^2 is the variance.

Before starting the main part of the algorithm, it is necessary to set a certain number of random values of parameters (uniform distribution of a random variable). After that the best point should be selected of all available coordinates (the best point is the coordinates at which the CF has an extreme value). The selected point is the first approach to the extremum. Then the random number generation with Gaussian distribution is used (expected value corresponds to the coordinates of the first approach, and the variance is still large). After each calculation of the CF for the next approach point, it is necessary to take the last point if the value of the CF of this point is the best among all. Thus, self-adaptation occurs by adjusting the expectation and reducing the variance (**Figure 1**). It should be noted that the dependence of the variance on the calculation number of the CF affects the optimization time.

Figure 1 is an example for the case if the limits for the variation by the optimized parameter were from 0 to 1 and the extremum would be located at the point with coordinates 0.55 for this parameter. After all the calculations of the function have expired, the last result (quasi-extremum) is taken as the result of optimization.

In order to make it convenient to depict the graphic dependence of the variance on the CF calculation number, we introduce the parameter T. It is the reciprocal for the variance σ^2

$$T = \frac{1}{\sigma^2}. \tag{2}$$

As stated above, before starting the main part of the algorithm, it is necessary to set a certain number of random values of parameters (uniform distribution of a

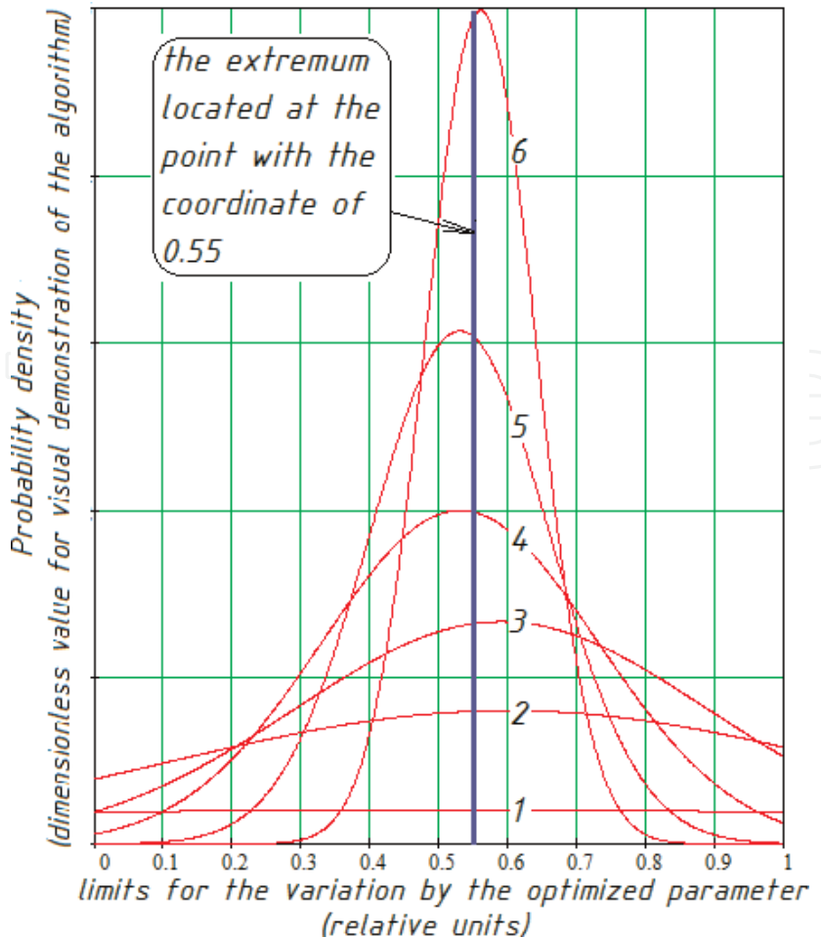


Figure 1.
Examples of probability density graphs (1, start of optimization; 6, completion of optimization).

random variable, variance value is high, T is close to zero). This will suggest that the global extremum will not be missed (familiarization zone, **Figure 2**). Next, self-adaptation should occur, and then a more accurate calculation of the extremum coordinates should follow. The dependence of the T on the CF calculation number is expressed as follows:

$$T(n_0) = k \cdot \frac{arctg(w \cdot n_0 - w \cdot S) + arctg(w \cdot S)}{arctg(w - w \cdot S) + arctg(w \cdot S)}, \tag{3}$$

where n_0 is the indicator of optimization completion, defined by Eq. (4), k is the coefficient that determines the value of the variance at the final stage of optimization (**Figure 3**), w is the parameter determining the duration of self-adaptation (**Figure 4**), and S is the parameter that determines when the self-adaptation will begin (**Figure 5**):

$$n_0 = \frac{n}{n_\Sigma}, \tag{4}$$

where n is the current calculation number of the CF and n_Σ is the total number of calculations of the CF (set before optimization).

Figures 3–**5** show the influence of parameters k, S, and w on the general form of the Eq. (3).

The analysis of **Figures 4** and **5** is presented in the form of **Table 1**.

As **Table 1** shows, various combinations of values can have both positive and negative effects. The values of S and w should be selected in such a way that the

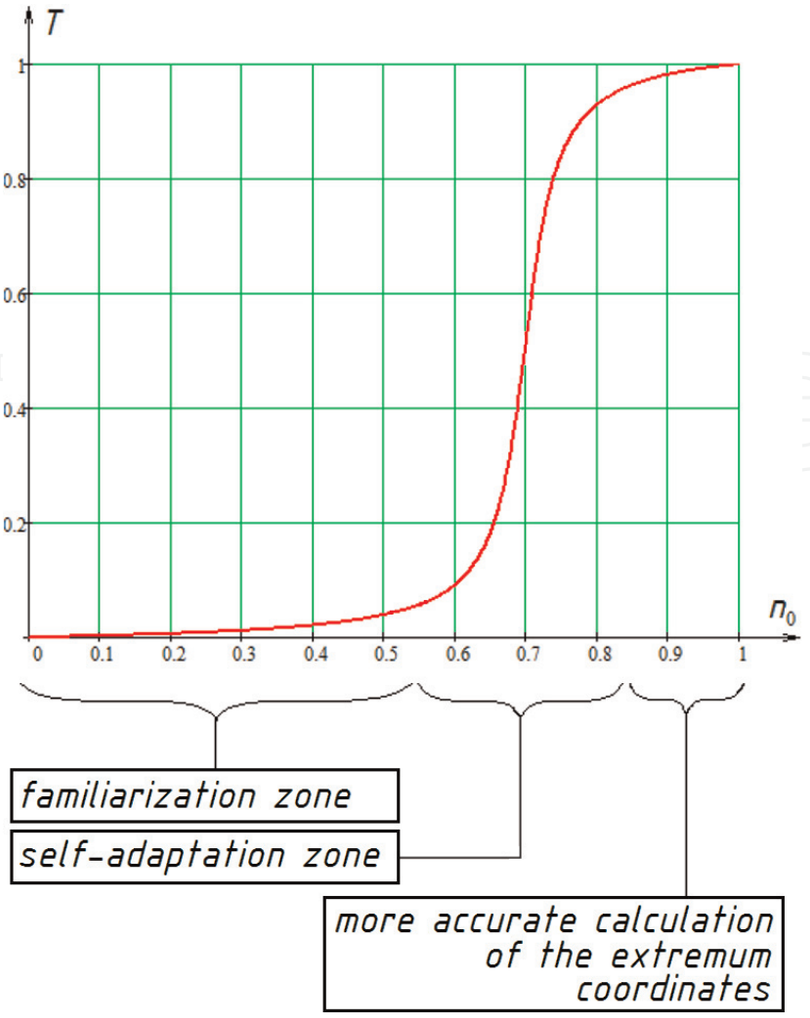


Figure 2.
The dependence of T (reciprocal for the variance σ^2) on the CF calculation number (k = 1; w = 30; S = 0.7).

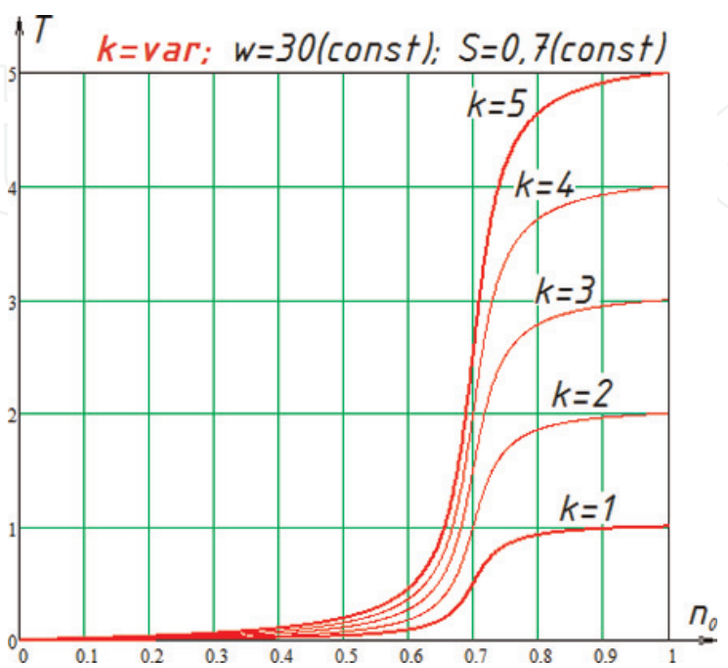


Figure 3.
The effect of parameter k on the general form of the dependence $T(n_0)$.

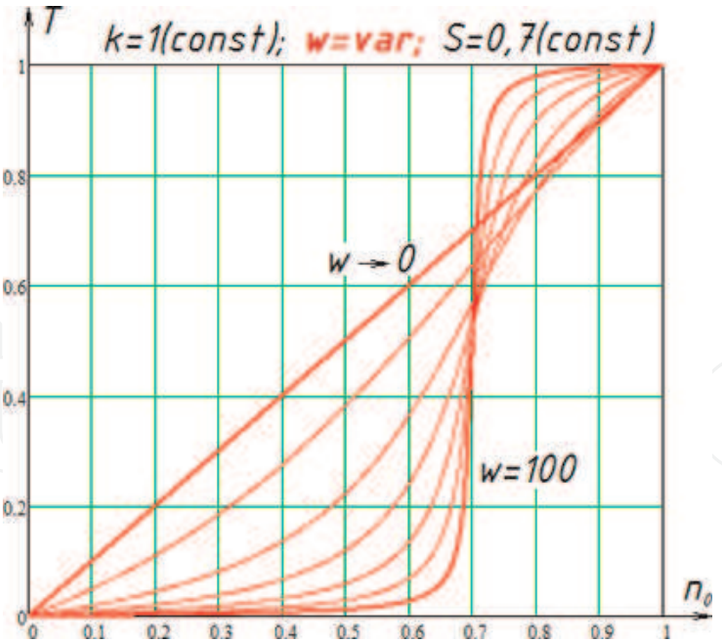


Figure 4.
The effect of parameter w *on the general form of the dependence* $T(n_o)$.

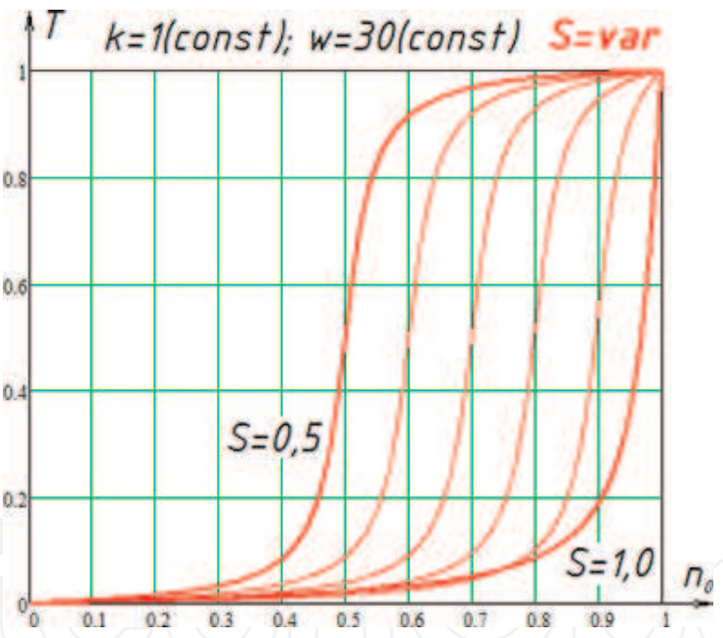


Figure 5.
The effect of parameter S on the general form of the dependence $T(n_o)$.

optimization result gives the greatest probability of finding a global extremum with the necessary accuracy. For different forms of CF, the best result will be given by different combinations of S and w. Therefore, the averaged values of S and w were found: S = 0.7 and w = 30 (**Figure 2**). These values were chosen empirically by multiple optimizations of test functions. The test functions were specified analytically. The coordinates of their extremum can be calculated without optimizing (to be able to assess the accuracy of finding a global extremum).

The coefficient k in Eq. (3) indicates the variance at the final stage of optimization (the accuracy of the extremum coordinates calculation).

The value of the coefficient k must be determined for each parameter being optimized separately. When optimizing the geometrical forms of the magnetic cores, this coefficient should be determined on the basis of the accuracy of the

	High value	Low value
S	*Positive effect:* • Increases the probability of finding a global extremum, rather than a local extremum	*Positive effect:* • Increases the number of CF calculations for more accurate calculation of the coordinates of the extremum
	Negative effect: • Decreases the number of CF calculations for more accurate calculation of the coordinates of the extremum	*Negative effect:* • Decreases the probability of finding a global extremum, rather than a local extremum
w	*Positive effect:* • Increases the probability of finding a global extremum, rather than a local extremum • Increases the number of CF calculations for more accurate calculation of the coordinates of the extremum	*Positive effect:* • Self-adaptation zone is increasing • Limitations in which the search for extremum which takes place can slowly narrow, so the real extremum will not be outside
	Negative effect: • Self-adaptation zone is reduced • Limitations in which the search for extremum which takes place can quickly narrow, leaving a real extremum outside (find it becomes impossible because the rapidity of variance reduction is large)	*Negative effect:* • Decreases the probability of finding a global extremum, rather than a local extremum • Decreases the number of CF calculations for more accurate calculation of the coordinates of the extremum

Table 1.
Analysis of the effect of parameters S and w on the result of optimization.

manufacturing equipment used in the manufacture of the SRM magnetic core. In addition, when determining the coefficient k, it is necessary to take into account the influence of each parameter value on the CF. Applied to SRM this question deserves special research [7].

When using the coefficient, it should be guided by the "68–95–99.7" rule: a random variable having a normal distribution does not deviate from the expectation in absolute value by more than 3σ with a probability of 99.73%.

The coefficient k should ensure the generation of random numbers at the final stage of optimization within limits equal to the limits of accuracy required (**Figure 6**).

The value of the coefficient should be determined by the following formula

$$k = \frac{1}{\sigma^2} = \frac{1}{\left(\frac{\delta}{3}\right)^2}, \tag{5}$$

where δ is the allowable relative error of extremum coordinates calculation.

Number 3 in the denominator indicates the value of three sigmas.

Eventually, the developed optimization algorithm was based on the distribution function with variable expectation and standard deviation (Eq. (6)). The expectation depends on the intermediate optimization results. The standard deviation and variance depend on the calculation number of the CF:

$$\begin{cases} f(x,\mu,n) = \dfrac{1 + erf\left(\dfrac{x-\mu}{\sigma(n)\sqrt{2}}\right)}{2}; \\ \sigma(n) = \left(\dfrac{2\cdot\delta}{6}\right)\sqrt{\dfrac{arctg(w - w\cdot S) + arctg(w\cdot S)}{arctg\left(w\cdot\dfrac{n}{n_\Sigma} - w\cdot S\right) + arctg(w\cdot S)}}, \end{cases} \tag{6}$$

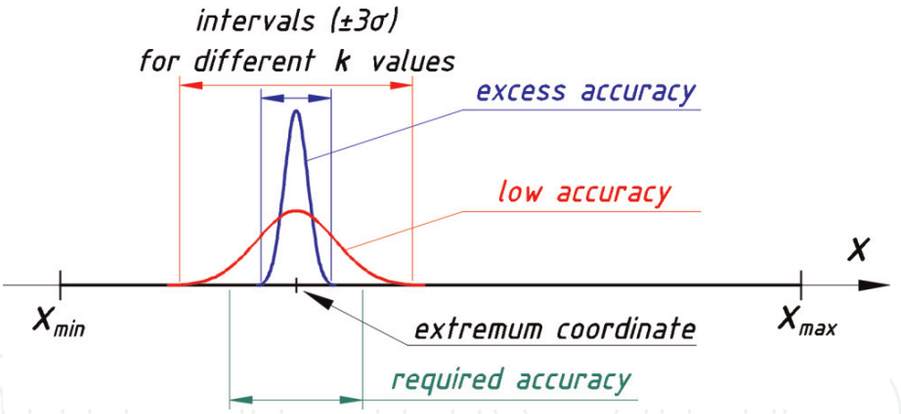


Figure 6.
The influence of the coefficient k on the accuracy of the extremum coordinates calculation.

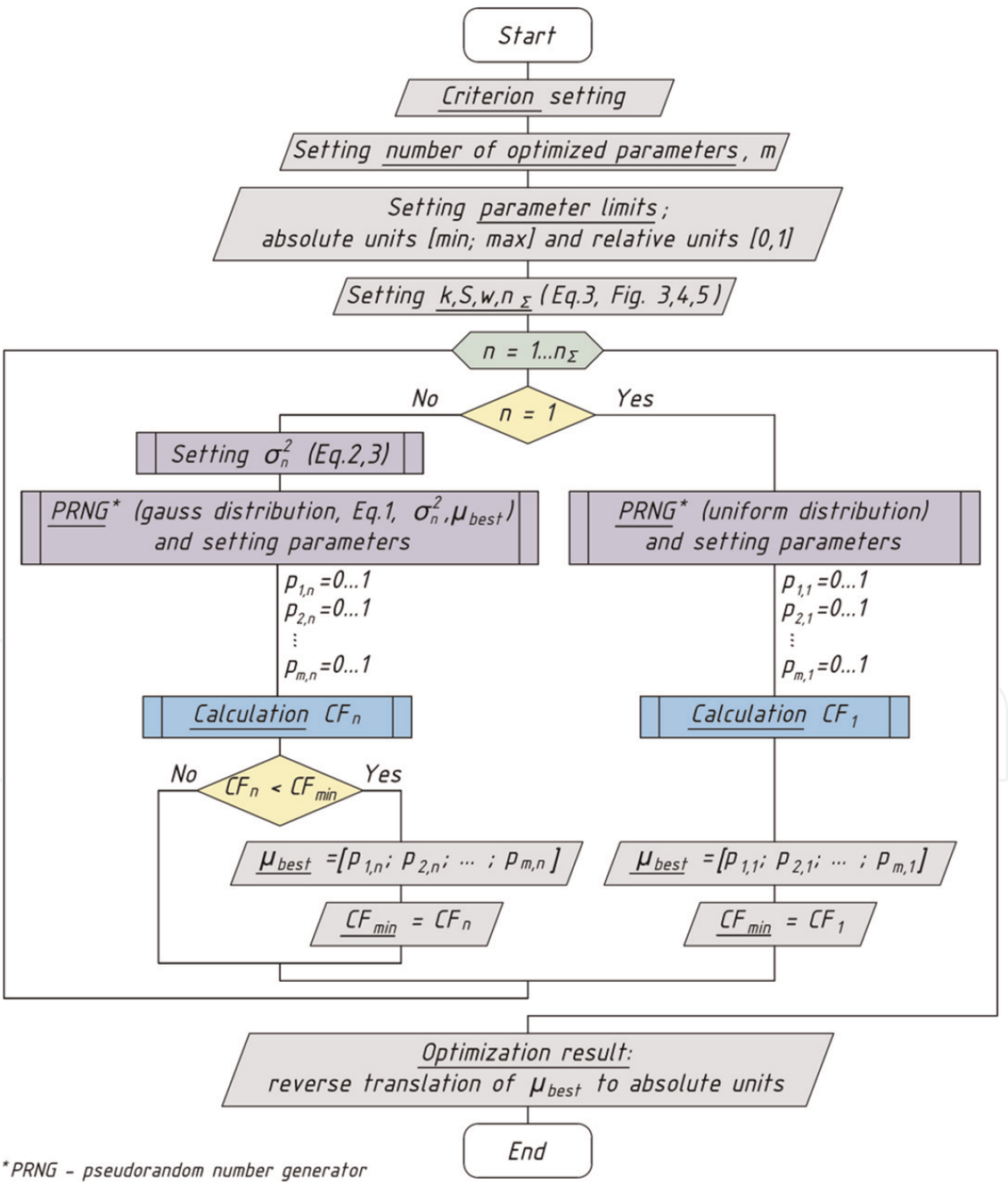


Figure 7.
Flowchart defining the developed optimization algorithm.

where $erf(x)$ is the Gauss error function (Eq. (7)) [8], μ is the expected value, $\sigma(n)$ is the standard deviation, n is the current calculation number of the CF, δ is the allowable relative error of extremum coordinates calculation, w is the parameter determining the duration of self-adaptation (**Figure 4**), S is the parameter that determines when the self-adaptation will begin (**Figure 5**), n_Σ is the total number of calculations of the CF:

$$erf\ (x) = \frac{2}{\sqrt{\pi}} \int_0^x e^{-t^2} dt. \tag{7}$$

Figure 7 summarizes Section 2 and shows the flowchart defining the developed optimization algorithm.

3. Mathematical description of the pole curved shape

When designing SRM, the shape of the poles of the rotor and stator is most often defined by contours similar to an isosceles trapezoid using segments and arcs [2, 9]. This results in a uniform air gap in the motor. **Figure 8** shows an example of the rotor pole contours (uniform air gap).

These restrictions on the shape of the magnetic core do not allow to fully realizing the possibilities for improving the performance of the SRM by changing the geometry of its magnetic circuit.

The scientific novelty of our research is the way of setting restrictions for varying the optimized geometric parameters of the SRM rotor by means of the zone shown in **Figure 9**.

As **Figure 9** shows, the location of the rotor pole contour is limited only by the diameter of the rotor shaft, the maximum approach to the stator, and the sector which depends on the number of poles of the rotor. The left side of the pole is set by mirroring the contours of the right side.

Note that it does not complicate the manufacturing technology, because modern equipment allows to make sheets of magnetic core without restrictions on their shape.

Consider the mathematical description of the rotor pole curved shape. When optimizing the geometry of the curved pole shape, it is necessary to generate a *random curve* at each step (**Figure 9**), in contrast to the optimization of the geometry of the trapezoidal pole shape (**Figure 8**), where it is necessary to generate *random numbers*, to setting specific geometric dimensions (b1r, b2r, etc.).

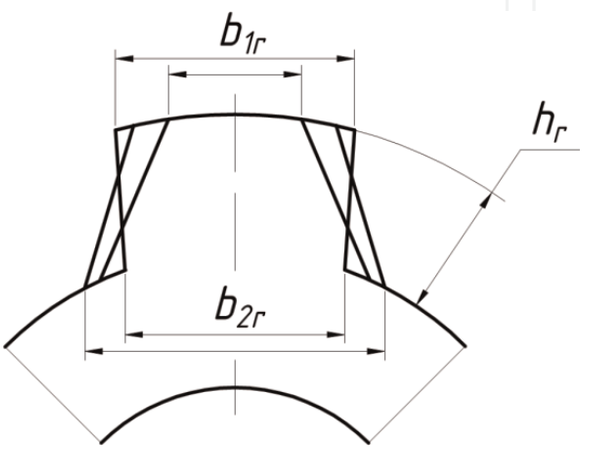


Figure 8.
Example of standard rotor pole defined using segments and arcs.

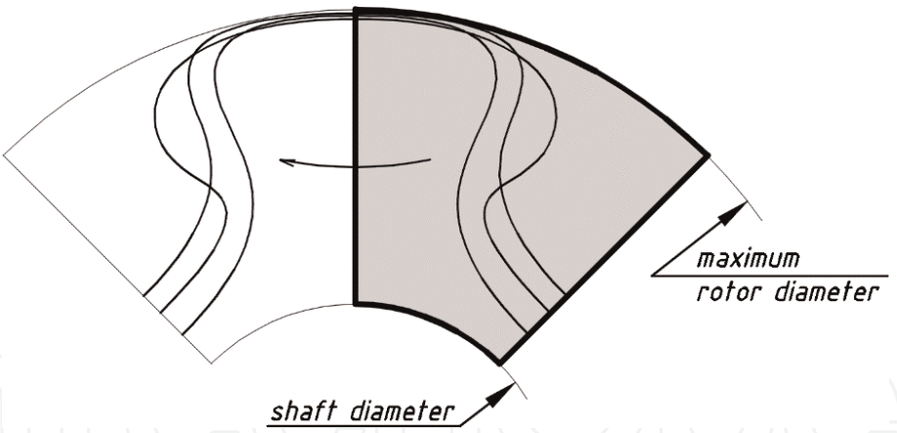


Figure 9.
The area of possible contours of the rotor poles when setting the curved shape of the pole.

To solve this problem, an algorithm for generating a random curve was developed. The design features of the SRM magnetic cores make it necessary to take into account some restrictions on the curve shape that determines the magnetic core at each step of optimization:

1. Point 1 (belongs to the pole contour and is located on the pole axis) must be farther from the rotor axis of rotation than point 2 (belongs to the pole contour and is located on the groove axis). This rule is shown in **Figure 10**.

2. The pole contour should not be in sharp protrusions, peaks, and other irregularities. This may degrade motor performance due to deep local magnetic saturation (**Figure 11**) [10].

3. To fulfill Eq. (2), it is necessary that on the border of the pole zone, the tangents to the magnetic core are perpendicular to the radial direction (**Figure 12**).

It is possible to take into account the above conditions if the random curve is set by means of the Cartesian coordinate system using the analytical formula, then bring the curve to the form required for the SRM pole (**Figure 13**).

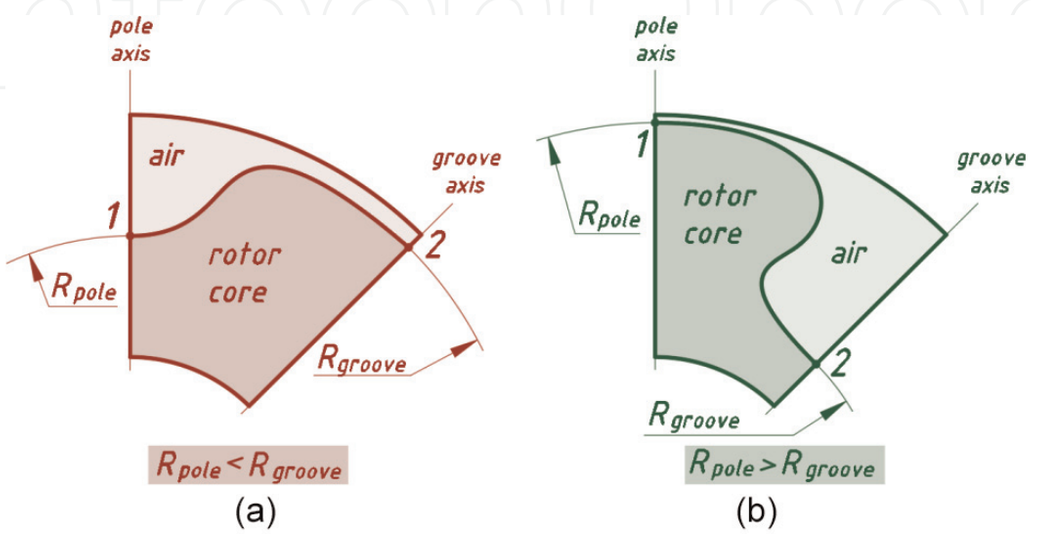


Figure 10.
An example of incorrect (a) and correct (b) setting of the coordinates of the boundary points of the pole contour.

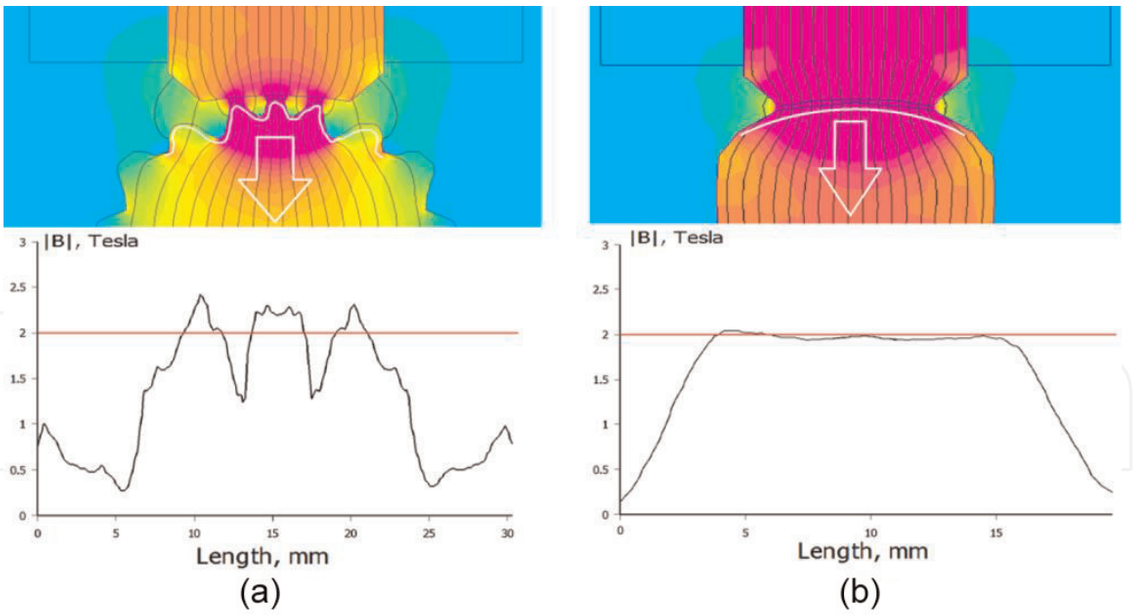


Figure 11.
An example of the influence of irregularities of the pole contour on the magnitude of the flux density in the magnetic core: incorrect (a) and correct (b) setting of the curve describing the pole contour.

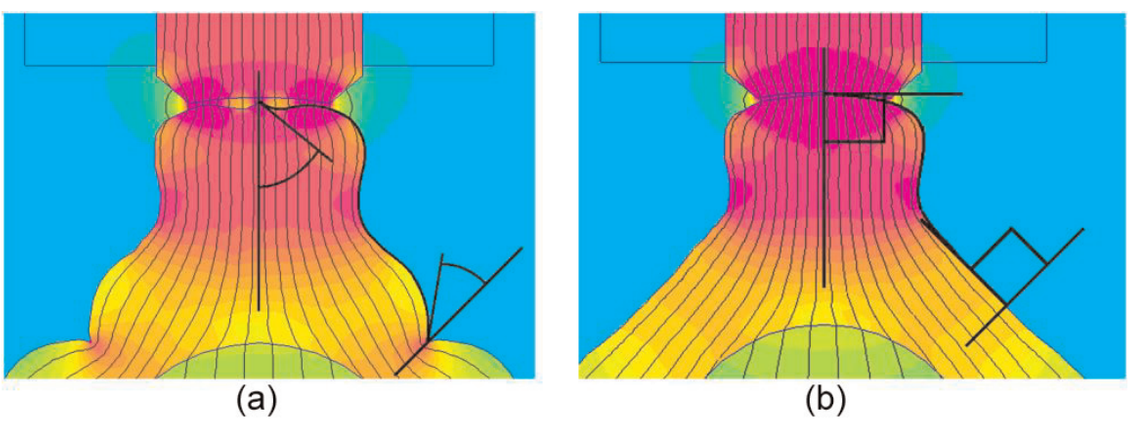


Figure 12.
Examples of incorrect (a) and correct (b) setting of the inclination of the extreme sections of the contour of the rotor pole.

Curve plotting condition: it should be located in the pole sector so that the segments (numbered from 1 to 21, **Figure 13b**) are separated by the curve in the same proportions as the corresponding segments in the Cartesian coordinate system (**Figure 13a**).

The proposed location of the segments (from 1 to 21) in the zone sector pole ensures Eq. (1) ($R_1 > R_2$, **Figure 10**).

To fulfill Eq. (2) (the pole contour should not be in sharp protrusions, **Figure 11**), it is advisable to set a random curve using the sum of sinusoids with different amplitudes, frequencies, and phases:

$$y_1(x) = \sum_{i=1}^{n} A_i \cdot \sin(\omega_i \cdot x + \varphi_i), \tag{8}$$

where n is the number of sinusoids, A is the amplitude, ω is the frequency, and φ is the sine wave phase.

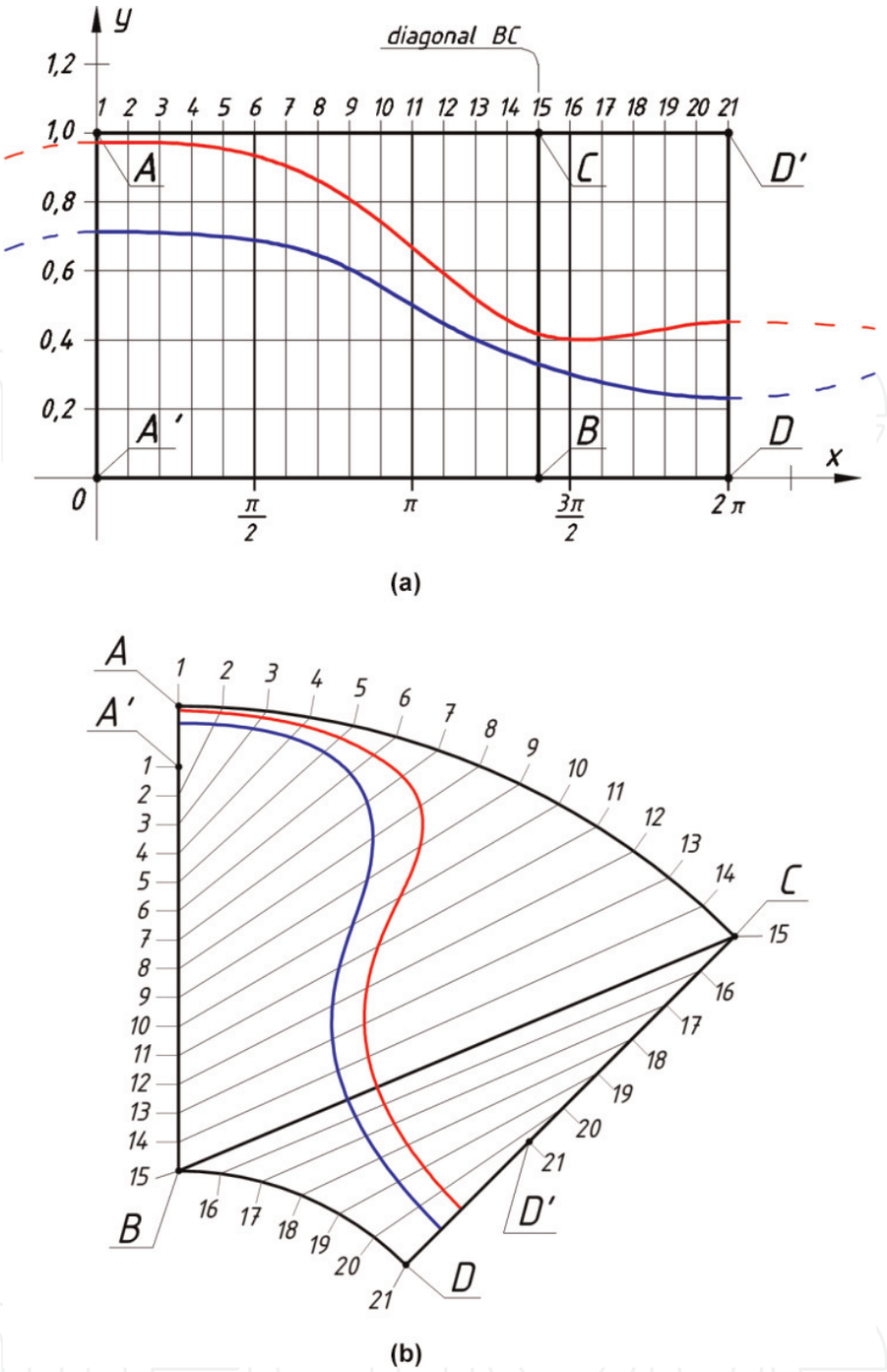


Figure 13.
The principle plotting of the rotor pole curved shape. The magnetic core curves (b) divide the segments (numbered from 1 to 21) in the same proportions as the corresponding initial curves (a) defined using a mathematical expression and represented in a Cartesian coordinate system.

As shown by the experience of designing SRM [11], in order to avoid protrusions and irregularities, the values n, A, and ω should be set as follows (**Table 2**).

To eliminate the irregularities of the magnetic core at the top of the pole and in the center of the groove (Eq. (3), **Figure 12**), it is necessary to further develop measures that exclude the inclination of the random curve in the abscissas 0 and 2π: the derivative in these coordinates should be zero, and this should not contribute to the appearance of high fluctuations on the curve. We write the equation of the curve as follows:

$$y_2(x) = \begin{cases} y_1(0) \cdot q(x) + y_1(x) \cdot (1 - q(x)), \text{if } x < \pi; \\ y_1(2\pi) \cdot q(x) + y_1(x) \cdot (1 - q(x)), \text{if } x \geq \pi, \end{cases} \quad (9)$$

Parameter name	Symbol	limitation		Value
		Min	Max	
Amplitude	A	0	1	0...1
Frequency	ω	0	1	0...1
Sine wave phase	φ	0	2π	0...2π
Number of sinusoids	n	—	—	2

Table 2.
Values of mathematical parameters of a random curve.

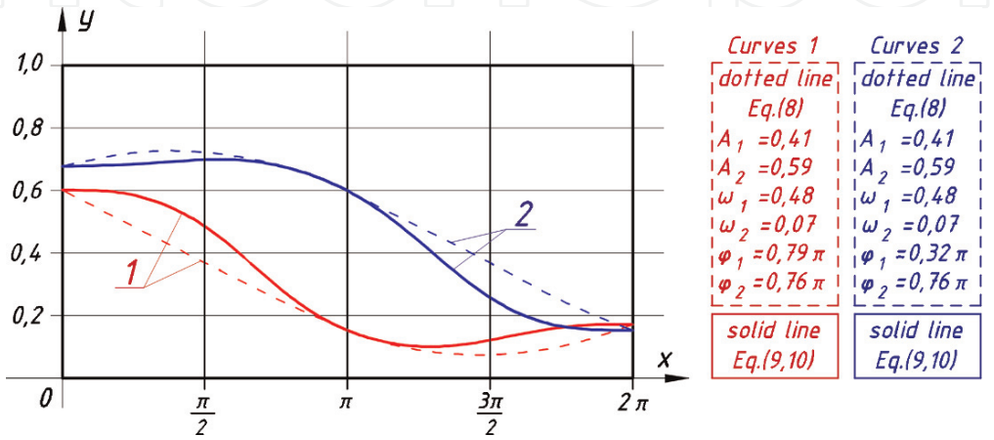


Figure 14.
Examples of changing the shape of curves after conversion (Eqs. (9) and (10)).

where $q(x)$ is the function that has value, $q(0) = 1$, $q(\pi) = 0$, and $q(2\pi) = 1$, and derivatives in these coordinates, $q'(0) = q'(\pi) = q'(2\pi) = 0$.

The most suitable for this is the equation:

$$\begin{cases} q(x) = \dfrac{\cos(x) + 1}{2}; \\ q'(x) = -\dfrac{\sin(x)}{2}. \end{cases} \tag{10}$$

The function values at the three significant coordinates ($x = 0$, $x = \pi$, $x = 2\pi$) remain unchanged after the conversion. The derivatives at boundary coordinates ($x = 0$ and $x = 2\pi$) become zero in the middle of this interval (for $x = \pi$); the derivative is equal to the derivative of the original function. This avoids the inclination of the curve in the boundary coordinates with a slight change in its shape compared to the original curve (**Figure 14**).

4. Optimization of the curved shape of the rotor pole

The above optimization algorithm is applicable to optimize the trapezoidal pole shape. To optimize the curved shape, it is necessary to take into account some features of the implementation of this algorithm in computer programming.

When optimizing the trapezoidal pole shape, the optimization parameters are clearly defined: they represent the specific geometric dimensions of the magnetic core. The curved shape of the pole does not have these geometric dimensions. The curved shape of the pole can be defined differently, for example, by the set of

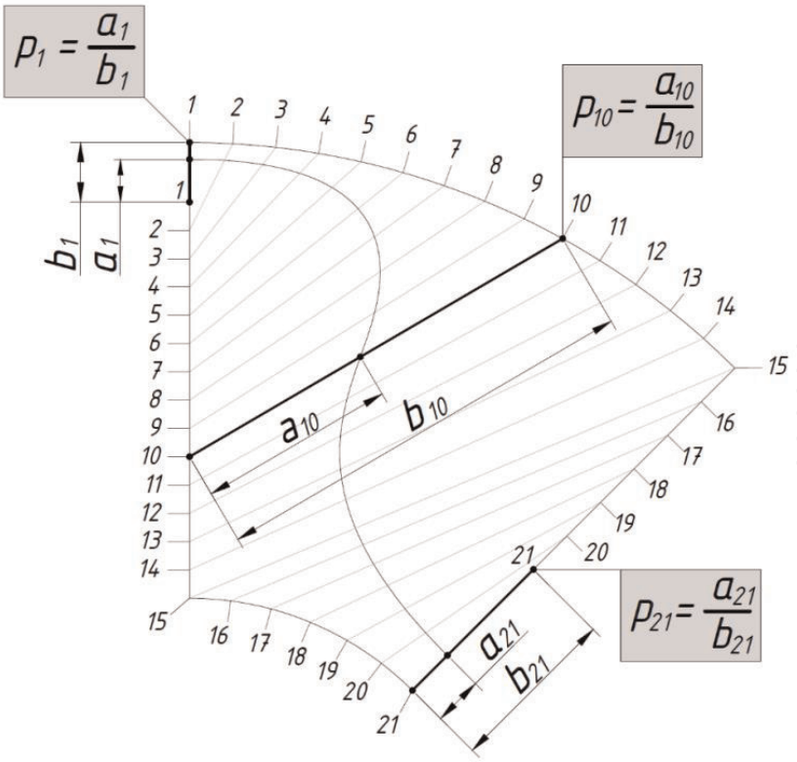


Figure 15.
Formation of optimization parameters and their values.

coordinates of the points belonging to this curve. Therefore, as optimization parameters, it is advisable to set the ratio (Eq. (11)) of the geometric dimensions a and b for each of the 21 segments (**Figure 15**).

$$p_n = \frac{a_n}{b_n}, \tag{11}$$

where p_n is the optimization parameter and a_n and b_n are the geometrical dimensions that determine the shape of the pole (**Figure 15**).

Thus, the number of optimization parameter is equal to the number of points defining the half-pole contour. It should be noted that an increase in defining points does not entail an increase in optimization time. The curve is set using six random numbers (for two sinusoids, as in our case) that are independent of each other, similarly, optimization by six parameters.

The number of defining points is selected for each design problem singly, depending on the required accuracy and smoothness of the pole contour. The number of defining points is limited only by the features of creating a mesh in a computer program for calculating magnetic fields (e.g., FEMM). The more points that define the pole, the more the number of nodes in the output mesh. This entails a significant increase in the calculation time without increasing their accuracy [12].

5. The example of optimizing the geometric shape of a rotor pole

As an example, consider the optimization of the curved shape of the rotor magnetic core for SRM 6/4; the outer diameter of the stator magnetic core is 131 mm, and the shaft diameter is 30 mm. The number of points defining the half-pole contour is 21.

Optimization criteria: minimum of torque ripple, it is defined as follows [4, 11, 13]:

$$\Delta T_e = \frac{\max(T_e) - \max(T_e)}{T_a} \cdot 100\%, \tag{12}$$

where ΔT_e is the torque ripple value (%), T_e is the instantaneous torque value (N m), and T_a is the average value of electromagnetic torque (N m).

When modeling electromagnetic processes in a SRM, the following assumptions were made:

1. The supply network has infinite power.
2. Losses in power switches and converter conductors are not taken into account.
3. Rotor eccentricity is absent; there is no deflection and shaft skew.
4. Magnetic field was calculated in two-dimensional space, calculated SRM space is stationary, and leakage flux at the end winding is neglected.
5. Electrical steel has isotropic properties for a two-dimensional computational space.
6. The shape of the current was rectangular (ideal case).

The result of the optimization is shown in the **Figure 16**.

In addition to the calculations, the electric motor with two rotors was tested alternately: with a rotor that was designed without the use of optimization methods and with a rotor whose geometric dimensions were obtained by optimization.

The purpose of the experiment was to obtain curves of the dependence of the torque on the rotor position for a motor with different rotor.

The experiment for each electric motor was carried out according to the following algorithm:

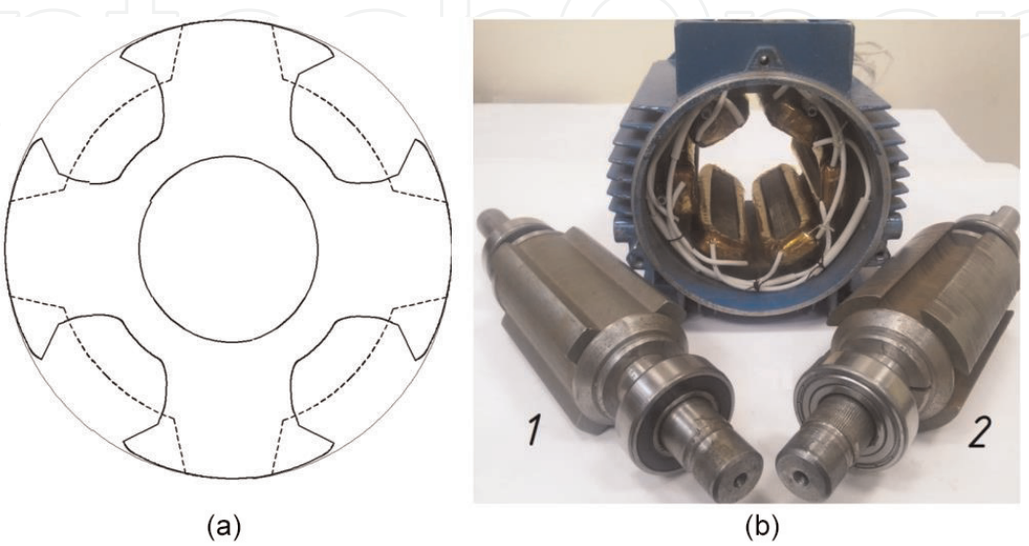


Figure 16.
Experimental SRM sample: 1 (dotted line) is the rotor obtained without optimization algorithm; 2 (continuous line) is the rotor obtained as a result of optimization.

- The values of the torque for the full rotation of the rotor were measured in 0.5° increments with a 0.33 m arm, at the end of which the strain gauge was attached. At the same time, the readings of two measuring instruments were registered: the absolute rotary encoder and the weight terminal (the force occurring in the strain gauge with an accuracy of 0.01 N). The phase windings were supplied with a variable autotransformer (with the help of which a current of 10 A), the diode bridge and a battery of capacitors with a total capacity of 4400 μF.

- According to the data, the curves of the dependence of the torque on the rotor position were obtained.

- The averaging of all sections of the curve, limited by the repeat interval, was performed. For a three-phase SRM, which has a 6/4 configuration, this interval is 30° (120 electric degree). Averaging of 12 sections was performed that correspond to different rotor positions. So, it was possible to reduce the error in measurements caused by the rotor eccentricity.

The results of the experiment are shown in **Figure 17**.

As can be seen from **Figure 17**, the experimental and calculated curves that correspond to one rotor are sufficiently close in form. When comparing the two experimental curves with each other, it follows that the torque ripple with the rotor obtained as a result of optimization is much less than for the motor with the rotor, which was designed without optimization. The torque ripple (Eq. (12)) with the rotor, which was designed without the use of optimization, is 137%. The torque ripple with the rotor, which was designed by means of optimization, is 51%. Thus, it was possible to reduce torque ripple more than 2.5 times.

When designing switched reluctance motors for specific applications, in addition to reducing the pulsations of the electromagnetic torque, other parameters, such as efficiency, thermal conditions, etc., need to be improved. To do this, we need to use a multi-objective optimization, for example, compiled using linear scalarization of cost function: The above optimization method based on Monte Carlo optimization method can also be used in the case of a multi-objective optimization:

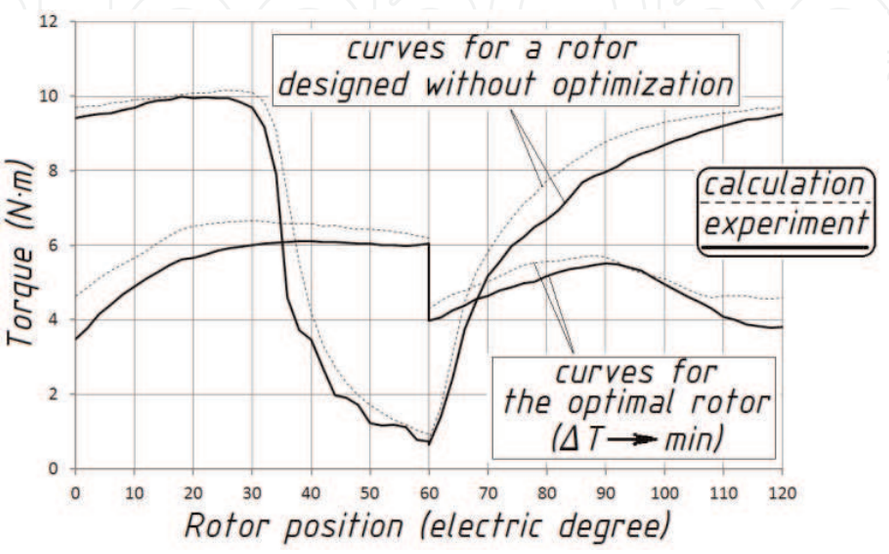


Figure 17.
Comparison of experimental results for two rotor samples.

$$F = \max\left(\sum_{i=1}^{k} w_i \cdot f_i(\overline{x})\right), \tag{13}$$

where F is the cost function of the optimization problem; k—number of optimization criteria; w_i is the weights of the objectives, which indicate the priority of the i-th criterion; and f_i is the function that depends on the values of the optimized parameters and indicates the numerical value of the i-th criterion.

The above optimization method based on Monte Carlo optimization method can also be used in the case of a multi-objective optimization.

Note that the design algorithm developed (allowing to get an uneven air gap and a curved pole shape) is applicable to optimize the stator pole. But for its implementation, it is necessary to take into account the additional restrictions that are created by the stator winding.

6. Development of the SRM optimal control algorithm

The following is one of the variants of the approach to the design of electric motors with regard to the control algorithm using the example of SRM, which are considered promising for applications.

It is known that the wider the range of permissible values of the coordinates and control actions of the control object, the less likely that the optimal dependence will pass along the boundary of the permissible values of coordinates or control actions and the greater the likelihood of obtaining a better final result. We formulate the requirements for the converter, which forms the control algorithm for the SRM on the basis that its functionality should be as wide as possible:

- To power one phase of the SRM, there must be at least one semiconductor key in order to be able to independently switch for this phase. The current must be supplied to the winding during the conduction interval set by the rotor position specified by the control algorithm, in order to ensure the specified operating mode.

- The converter should be able to regulate the phase current in the whole range of frequencies of rotation of the SRM and form a predetermined form of current using pulse-width modulation (PWM) together with frequency-pulse modulation (FPM).

- The converter should be able to simultaneously feed several phases independently of each other, as well as ensure the operation of phases with overlapping.

As a converter for powering SRM, we use the most common half-bridge circuit. Various control laws can be implemented using modulation of the supplying voltage of the SRM and forming a current wave of almost any shape in the stator winding.

Find the power supply parameters of the SRM, which will provide a minimum of cost function, the integrand of which includes the square of the voltage applied to the stator winding:

$$J_\Phi = \int_{\theta 1}^{\theta 2} \frac{u^2}{R} d\theta \tag{14}$$

The optimization criterion is selected based on the analysis of variables affecting electrical losses. The integrand (Eq. (14)) determines the electrical losses according to the Ohm's law for linear electrical circuits (containing only active elements). In SRM, the relationship between current and voltage is nonlinear, and the integrand (Eq. (14)) is not identical to electric losses. In spite of this, minimization (Eq. (14)) can significantly reduce the electrical losses in the stator SRM, as shown by calculations.

In solving the problem of optimal control, the maximum principle is used. The equations for the SRM parameters, auxiliary ψ-functions, and the optimal control action u^* are

$$\begin{cases} \dfrac{di_a}{d\theta} = \dfrac{1}{\omega \cdot Z_p \cdot L} \cdot \left(u - i_a R - i_a \cdot \omega \cdot Z_p \cdot \dfrac{dL}{d\theta} \right) \\ \dfrac{d\omega}{d\theta} = \dfrac{1}{J \cdot \omega \cdot Z_p} \cdot \left(\dfrac{Z_p \cdot i_a^2}{2} \dfrac{dL}{d\theta} - T_R \right) \\ \dfrac{d\psi_1}{d\theta} = \psi_1 \left(\dfrac{R}{L \cdot \omega \cdot Z_p} + \dfrac{1}{L} \dfrac{dL}{d\theta} \right) - \dfrac{i_a \cdot \psi_2}{J \cdot \omega} \dfrac{dL}{d\theta} \\ \dfrac{d\psi_2}{d\theta} = \dfrac{\psi_1}{L \cdot \omega^2} (u - i_a R) + \dfrac{\psi_2}{J \cdot \omega^2} \left(\dfrac{i_a^2}{2} \dfrac{dL}{d\theta} - T_R \right) \\ u^* = \dfrac{\psi_1 \cdot R}{2 \cdot L \cdot \omega \cdot Z_p} \end{cases} \tag{15}$$

where θ is the rotation angle of the rotor, ω is the angular frequency of shaft rotation, Z_p is the number of salient poles on the rotor, i_a is the stator phase current, R is the resistance of the stator winding, L is the inductance of the stator winding, J is the moment of inertia of the rotor and the mass of the executive mechanism attached to it, and T_R is the torque of resistance on the motor shaft.

The first equation (system of Eq. (15)) is based on the Kirchhoff's voltage law for one phase of the SRM. The second equation is the power balance equation (Cauchy equation): dynamic torque, electromagnetic torque, and torque of resistance. The remaining equations are obtained from the auxiliary function H according to the maximum principle:

$$H = \psi_1 \left(\frac{1}{\omega Z_p L} (u - i_a R) - i_a \omega Z_p \cdot \frac{dL}{d\theta} \right) + \psi_2 \left(\frac{1}{J \omega Z_p} \left(\frac{Z_p \cdot i_a^2}{2} \cdot \frac{dL}{d\theta} - T_R \right) \right) - \frac{u^2}{R}; \tag{16}$$

$$\frac{d\psi_1}{d\theta} = -\frac{\partial H}{\partial i_a}; \tag{17}$$

$$\frac{d\psi_2}{d\theta} = -\frac{\partial H}{\partial \omega}; \tag{18}$$

$$u^* = \frac{\partial H}{\partial u}. \tag{19}$$

The initial values of the auxiliary functions were found using the Newton-Raphson iteration method based on the following equation:

$$\begin{bmatrix} \psi_1(t_0)^{j+1} \\ \psi_2(t_0)^{j+1} \end{bmatrix} = \begin{bmatrix} \psi_1(t_0)^j \\ \psi_2(t_0)^j \end{bmatrix} - \begin{bmatrix} \dfrac{\partial i_a(t_{end})}{\partial \psi_1(t_0)^j} & \dfrac{\partial i_a(t_{end})}{\partial \psi_2(t_0)^j} \\ \dfrac{\partial \omega(t_{end})}{\partial \psi_1(t_0)^j} & \dfrac{\partial \omega(t_{end})}{\partial \psi_2(t_0)^j} \end{bmatrix}^{-1} \times \begin{bmatrix} i_a(t_{end}) - i_{a/end} \\ \omega(t_{end}) - \omega_{end} \end{bmatrix}, \tag{20}$$

where j = 1, 2... is the iteration number, $\psi_1(t_0)$ and $\psi_2(t_0)$ are the initial values of auxiliary functions, $i_a(t_{end})$ and $\omega(t_{end})$ are the stator winding current and the angular frequency of rotation of the rotor at the j-th iteration at the end of the integration interval at $t = t_{end}$, and $i_{a/end}$ and ω_{end} are the desired values of the stator winding current and the angular frequency of rotation of the rotor at the end of the integration interval (boundary conditions).

More detailed mathematical transformations to obtain the solutions to Eqs. (15) and (20) are given in [3, 14].

The calculations selected SRM with the following initial data: number of salient poles on the stator, 6; number of salient poles on the rotor, 4; phase resistance at 20°C, 0.4 Ω; number of phases, 3; stator package length, mm, 80; outer diameter of the stator, mm, 131; height of salient poles on the stator, mm, 21.2; width on the stator and rotor salient poles on the side of the air gap, mm, 8.8; stator core height, mm, 8.2; height of the rotor core, mm, 4.4; and inner diameter of the rotor core (shaft diameter), mm, 73.70.

In the practical application of SRM, there are always restrictions on the amplitude of the supply voltage. **Table 3** shows the calculation results for the three options. Three different options are selected from the condition of limiting the voltage in the DC link: for the first option, the voltage is not more than 325 V, for the second option, the voltage is not more than 415 V, and for the third option, the voltage is not more than 566 V.

To correctly compare the magnitude of the electrical losses over the switching period, calculations were performed for the same average value of the electromagnetic torque of all three options.

In the calculations, restrictions were imposed on the amplitude of the supply voltage, so that the parameters of the SRM and the supply converter did not exceed the maximum permissible values. In option 1 (**Figure 18**), a voltage pulse of constant amplitude was applied to the SRM stator winding—an option without optimization. Options 2 and 3 are calculated by the optimization criterion (Eq. (14)) with different voltage limits. For the calculation of option 1 and 3, the voltage value is chosen on the basis that the primary source of voltage for the converter is an industrial AC main voltage of 230 and 400 V, respectively. In carrying out the calculations of option 2, an intermediate nonstandard value was taken to illustrate the tendency of the SRM power parameters to change.

As can be seen from the **Table 3**, the electric losses in the stator winding with the optimal form of the supply current are significantly reduced, and the higher the voltage limit, the lower the electrical losses. From **Figure 18** it can be seen that the current I_3, corresponding to the lowest electrical losses, is characterized by a decrease in the amplitude value at the beginning of the switching process and a higher value of the current in the middle of the switching cycle with respect to the rest of the current curves.

Figure 18 shows the power supply interval of the phase winding. The optimal control problem was solved at this interval. The end of this interval corresponds to the moment of power off. The graphical dependencies of the currents I_1 and I_3

No.	U_{max}, V	ΔP (el. loss), %	I_{max}, A	T_a, N·m
1	325	100	31.8	7.7
2	415	84.5	25.9	7.7
3	566	74.1	21.0	7.7

Table 3.
The calculation results for the three options.

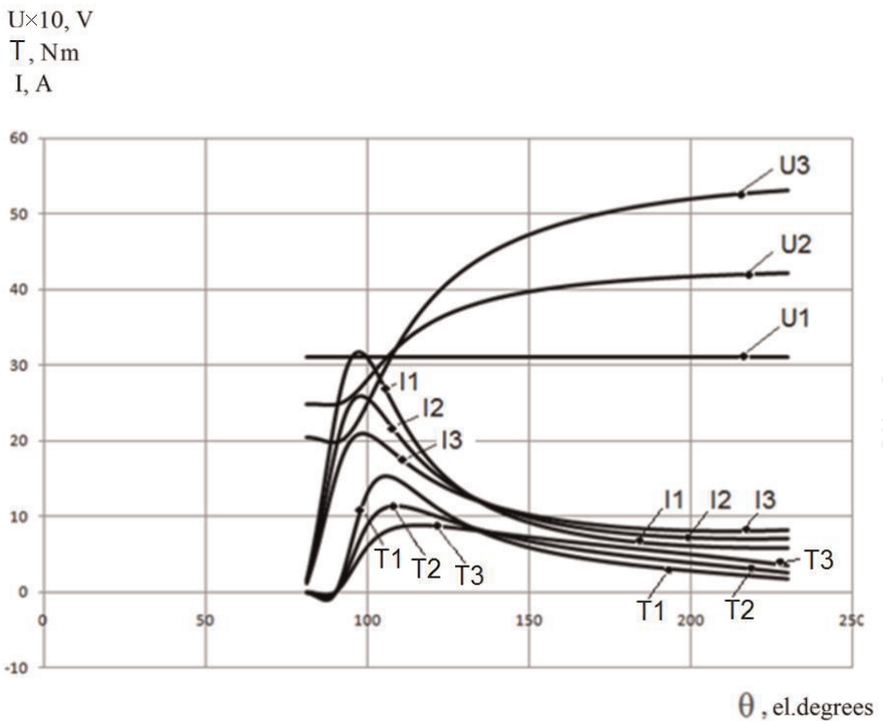


Figure 18.
Curves of changes in the parameter SRM during the controlled switching process, in which the stator winding is under the supply voltage.

versus rotor position (**Figure 19**) show the total current flow interval in the winding, including active interval (voltage applied to the winding) and passive interval (voltage is not applied to the winding, but the energy stored in the winding is returned to the source through the return diodes of the half-bridge power supply circuit). At the optimal variant of the change in current after a power failure, the current decreases faster due to the higher reverse voltage applied to the winding.

Practical implementation of algorithms for optimal control SRM.

Currently, there are a number of options for the formation of the optimal dependence of current on time. It seems rational to use PWM together with FPM, just as for an asynchronous motor, a current form is formed that approximates a sinusoid with PWM. To obtain maximum current repetition of the desired shape of the curve, the number of sampling points of current dependence on time increases, while the maximum pulse duration is reduced, and their frequency is increased with the help of PFM. FPM is used to obtain an optimal SRM current graph, since SRM has a nonlinear current dependence on the rotation angle and rotation frequency, and this in turn imposes limitations on the time of current rise in the SRM phase. From the beginning of each phase SRM to its end, the switching frequency of the half-bridge transistors should constantly change, taking into account the geometric design features of the active part SRM, as well as the specified characteristics. It is also necessary to implement with the help of PWM intermediate current increments that provide a smooth transition from one switching frequency of transistors to another, as well as provide protective and restrictive functions. In practice, all the necessary SRM parameters are read by the control converter as follows:

Phase current is obtained by digitizing an analog signal, a matched level, and certain limits, from a current transformer or a galvanically isolated shunt connected in series with each phase of the SRM.

Voltage is obtained by digitizing the analog signal, the agreed level, and certain limits, from the voltage divider galvanically isolated using linear optocouplers.

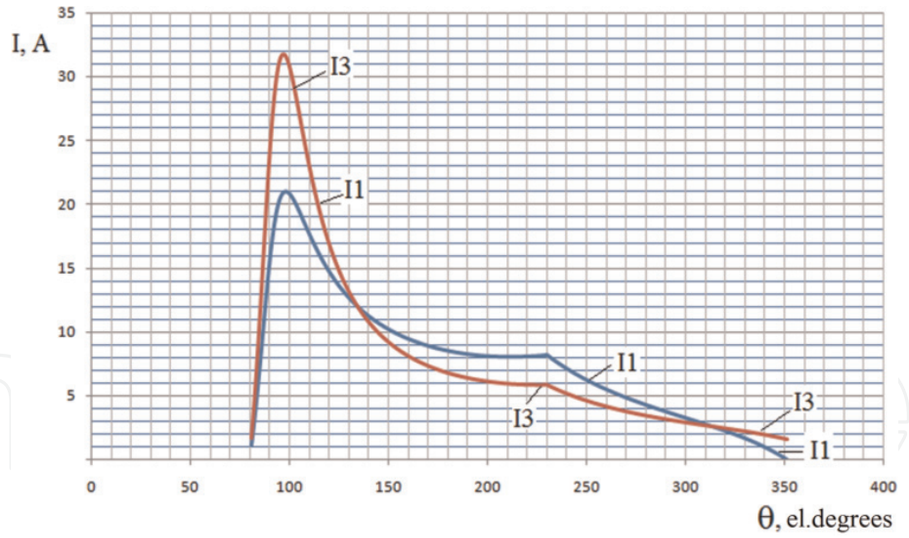


Figure 19.
Chart currents for the full switching cycle of a single-phase SRM.

The rotation angle of the rotor is read from the encoder (both incremental and absolute encoders can be used), and it can also be obtained by processing test pulses sent to the SRM phase (without encoder control system).
The binding of the obtained parameters to the time is carried out by the timers-counters of the microcontroller used to control the SRM.

One of the microcontroller control subroutines solves Eqs. (15) and (20) based on the ADC data obtained using the built-in DMA controller (direct memory access controller). Of course, the microcontroller subprogram solves Eqs. (15) and (20) not in the form presented by the formulas; otherwise it would not have time to process them in time, but in a program-logical form, where the variables of Eqs. (15) and (20) are read and their limits are given. In this case, the entire calculation process takes place in one of the real-time systems such as FreeRTOS or TNKernel. The use of such operating systems helps to properly prioritize and sequence actions when collecting data on the SRM and calculating the sequence of control pulses to obtain the optimal current curve in real time.

Before the microcontroller program issues a sequence of control pulses to the SRM phase control driver, it goes through several stages:

Input of parameters and desired characteristics SRM into the EEPROM of the microcontroller from the interface panel of the configuration
Obtaining parameters SRM using ADC and encoder
Binding of the obtained data to time using timers-counters in the real-time operating system
Setting event flags and reading automatically changing event registers
Simultaneous reading of the time intervals of the components of the process of measuring all parameters and calculating the characteristics SRM over a period of time due to the preset sampling of the angle of rotation and the current rotor speed calculated by the difference in time between the encoder pulses relative to the set reference flags or registers
After receiving and calculating all unknowns in Eqs. (15) and (20), the microcontroller program selects the desired sequence and duration of control pulses to realize the desired current shape depending on the preset limits of parameters and desired characteristics of the SRM.

Even with the achievement of a correctly written program for the microcontroller and the optimization calculation of the SRM geometry, there will always be restrictions for their implementation related to the component base of the converter control. First of all, this refers to the semiconductor elements IGBT and MOSFET. Until recently, IGBT for SRM phase switching was the most popular, because they have small gate capacitances and a short recovery time of the free-wheel diode when switching high currents and voltages, as compared with MOSFET of the same price category. Their only drawback is that the switching frequency is up to 100 kHz, which imposes a restriction on the discretization of pulses forming a SRM current curve. At the moment, the markets appeared are MOSFET, Wolfspeed, and CREE [15]. MOSFET data have zero tail current. Along with this, Wolfspeed produces Schottky SiC diodes with zero reverse recovery current. By using a Z-FET™ and MOSFET™ bundle with Z-Rec™ Schottky diodes, you can get "all-SiC" high-power switching circuits. The switching frequency of such a MOSFET bundle is limited by the maximum operating frequency of the driver and, that, in turn, is limited by the response time of the galvanic isolation circuit. Although these limitations exist, using drivers with a large inverse gate-source current and implementing a driver power supply circuit with a bipolar power source, as well as minimizing parasitic capacitances and inductances in the control circuit of the power transistors during PCB layout, they can be removed completely. The microcontroller operates at large switching frequencies and is not taken into account as a limiting factor for the implementation of the program for the formation of optimal SRM current curves.

The use of optimal SRM control by optimization criterion (Eq. (14)) allowed to significantly reduce electrical losses in the winding.

In practice, the optimal control of the SRM can be realized with the help of shared pulse-width and pulse-frequency modulation, supplemented by a high-speed data acquisition system for the microcontroller.

The derivation of control laws and formulas for calculating the driving pulses that form the optimal SRM current graph for each of its possible operation modes and performance ranges is achieved in practice by a microcontroller control program generating these pulses according to conditions that are initially determined based on the optimal control problem, by means of collecting and calculating all unknown equations of the mathematical model of SRM in real-time systems.

7. Conclusions

Optimization algorithms used at different stages of the SRM life cycle (design, manufacturing, exploitation, recycling) can significantly improve all technical and economic performance of the SRM including environmental issues, loss reduction, and reduction of energy costs in the performance of certain work.

Further development of this line of research will consist in the fact that the optimization problem will be solved in a more general formulation and eventually will cover the entire life cycle of SRM, as a converter of one type of energy into another.

DOI: http://dx.doi.org/10.5772/intechopen.89123

IntechOpen

IntechOpen

Author details

Petrushin Alexandr Dmitrievich*, Kashuba Alexandr Viktorovich
and Petrushin Dmitry Alexandrovich
Rostov State Transport University, Rostov-on-Don, Russia

*Address all correspondence to: alex331685@yandex.ru

IntechOpen

© 2020 The Author(s). Licensee IntechOpen. Distributed under the terms of the Creative Commons Attribution - NonCommercial 4.0 License (https://creativecommons.org/licenses/by-nc/4.0/), which permits use, distribution and reproduction for non-commercial purposes, provided the original is properly cited. BY–NC

References

[1] Krishnan R. Switched Reluctance Motor Drives. Modeling, Simulation, Analysis, Design and Applications. Boca Raton: CRC Press; 2001. DOI: 10.1201/9781420041644

[2] Miller TJE. Switched Reluctance Motors and their Control. Oxford: Magna Physics Publishing and Clarendon Press; 1993. 205p

[3] Petrushin AD. Energy Saving Switched Reluctance Drives and Asynchronous Drives for an Electric Rolling Stock. Rostov-on-Don: Publishing House of the North Caucasus Scientific Center of Higher Education; 1999. 72p

[4] Petrushin AD, Shcherbakov VG, Kashuba AV. Magnetic system optimization of switched reluctance motor. Russian Electromechanics. 2017; **1**:20-27. DOI: 10.17213/0136-3360-2017-1-20-27

[5] Rastrygin LA. Adaptation of Complex Systems. Riga: Zinatne; 1981. 375p

[6] Himmelblau DM. Applied Nonlinear Programming. New York: McGraw-Hill; 1972. 498p

[7] Shevkunova AV. Study of influence of fragments of magnetic system of a switched-reluctance motor on the average value of electromagnetic torque. Vestnik RGUPS. 2016;**3**:116-123

[8] Bronshtein IN, Semendyayev KA. Math Handbook. Moscow: Nauka; 1986. 544p

[9] Radimov IN, Rymsha VV, Procina ZP. Pole overlaying coefficients of a three-phase switched-reluctance motor. Electrical and Electrical Engineering. 2009;**73**:63-67

[10] Kopylov IP. Electric Motor Design. 4th ed. Moscow: Urait; 2012. 767p

[11] Petrushin AD, Kashuba AV. Improvement of switched reluctance motor performance using optimization algorithms. In: Proceedings of 10th International Conference on Electrical Power Drive Systems ICEPDS 2018; October 3–6, 2018; Novocherkassk: IEEE; 2018. pp. 3-6

[12] Meeker D. Finite Elements Method Magnetics. Version 4.2. User's Manual (FEMM4.2). California, USA; 2013. 161p

[13] Petrushin AD, Kashuba AV. Optimization of the magnetic system of switched reluctance motor. Vestnik RGUPS. 2016;**1**:61-65

[14] Petrushin AD. Energy-saving drives of electric rolling stock based on switched reluctance and induction electric motor [thesis]. Rostov State Transport University, Rostov-on-Don, Russia

[15] SiC and GaN Power and RF Solutions. Wolfspeed [Internet]. 2019. Available from: https://www.wolfspeed.com/ [Accessed: 26 May 2019]